International Journal of Thermophysics, Vol. 25, No. 4, July 2004 (© 2004)

Radiance Temperatures and Normal Spectral Emittances (in the Wavelength Range of 1500 to 5000 nm) of Tin, Zinc, Aluminum, and Silver at Their Melting Points by a Pulse-Heating Technique[1]

K. Boboridis,[2,3] A. Seifter,[2] A. W. Obst,[2] and D. Basak[4]

The radiance temperatures at four wavelengths (in the range of 1500 to 5000 nm) of tin, zinc, aluminum, and silver at their respective melting points were measured by a pulse-heating technique using a high-speed fiber-coupled four-wavelength infrared pyrometer. The method is based on rapid resistive self-heating of a sample from room temperature to its melting point in less than 1 s while measuring the radiance emitted by it in four wavelength bands as a function of time. A plateau in the recorded radiance-versus-time traces indicates melting of the sample. The melting-point radiance temperatures for a given sample are determined by averaging the measured temperatures along the plateau at each wavelength. The melting-point radiance temperatures for each metal are, in turn, determined by averaging results for several samples. The normal spectral emittances at the melting transition of each metal are derived from the measured radiances at each wavelength and the published values of the thermodynamic (true) melting temperatures.

KEY WORDS: aluminum; emissivity; emittance; melting; radiance temperature; silver; tin; zinc.

[1]Paper presented at the Fifteenth Symposium on Thermophysical Properties, June 22–27, 2003, Boulder, Colorado, U.S.A.

[2]Physics Division, P–23, MS H803, Los Alamos National Laboratory, Los Alamos, New Mexico 87545, U.S.A.

[3]To whom correspondence should be addressed. E-mail: kboboridis@fastmail.fm

[4]Metallurgy Division, National Institute of Standards and Technology, Gaithersburg, Maryland 20899, U.S.A.

0195-928X/04/0700-1187/0

1. INTRODUCTION

In the past three decades high-speed radiation thermometry, more commonly referred to as pyrometry, has been used extensively in conjunction with a pulse-heating technique to measure thermophysical properties of metals and alloys at high temperatures. In the course of these investigations at the thermophysics laboratories of the U.S. National Institute of Standards and Technology (NIST) and its Italian counterpart, the Instituto di Metrologia 'G. Colonnetti' (IMGC), it was noted that the radiance temperatures near 0.65 and 1 μm of several metals at their melting points are highly reproducible and independent of the initial surface roughness of the sample. This led to the suggestion [1] that the melting-point radiance temperatures of selected metals be used as secondary high-temperature reference points for high-speed pyrometry. The radiance temperature of a metal at its melting point depends on the operating wavelength of the measuring instrument. Hence, in order to establish such secondary reference points, an accurate knowledge of the wavelength dependence of the melting-point radiance temperatures of the selected metals would be required. Since high-temperature pyrometry is generally concerned with temperatures exceeding 1000 K, the wavelength range of interest was 400 to 1000 nm, that of silicon detectors. A six-wavelength pyrometer, operating in the nominal range of 500 to 900 nm, was constructed at NIST [2] and an effort was initiated to study as many of the high melting point metals as possible [3–6]. These measurements were later extended to longer wavelengths with the addition of a channel operating at 1500 nm [7–10].

Since then, continued advances in infrared detector technology have made high-speed pyrometric measurements feasible at much lower temperatures. At the Los Alamos National Laboratory (LANL) we have recently developed a high-speed four-wavelength infrared pyrometer for measurements on shock-compressed solids. These measurements provide valuable constraints on the equations of state of materials. In an effort to validate the new pyrometer, as well as the technique we use to determine true temperature from the measured radiances in the absence of a simultaneous emittance measurement [11], we used the NIST pulse-heating system to look at the melting transition of several metals. These metals were chosen to adequately cover the useful measurement range of our pyrometer with their melting points. In this paper we report our results on the melting-point radiance temperatures of tin, zinc, aluminum, and silver at four wavelengths in the range of 1500 to 5000 nm. We also report their normal spectral emittances as computed from the measured radiances at their melting points and their well-known (true) melting temperatures. In a sense, this is a continuation of the work that has been carried out at

the NIST and the IMGC over the last few decades and at the same time extends it to lower temperatures and longer wavelengths.

2. MEASUREMENT METHOD AND SYSTEM

The measurement technique is based on rapid resistive self-heating of a sample from room temperature to its melting point in less than one second by the passage of a large electrical current pulse through it. The radiance temperatures of the sample at the wavelengths of interest are measured during heating as a function of time. A plateau in the recorded radiance-versus-time traces indicates melting of the sample.

2.1. Pulse-Heating System

The pulse-heating system consists of the sample in series with a battery bank, an adjustable resistor, and a computer-controlled solid-state switch. The sample is mounted inside a vacuum chamber with several ports for optical measurements. To allow measurements in the mid-infrared spectral region, we used a CaF_2 window, instead of the typical BK7 window, in the pyrometry port. The battery bank voltage and the setting of the adjustable resistor determine the heating rate of the sample. Details regarding the construction and operation of the pulse-heating circuit are given elsewhere [12–14].

2.2. Radiometric System

The new LANL pyrometer consists of two separate units, a front-optics unit and a detector unit, that are linked with an optical fiber. This modular design offers flexibility in the choice of front optics that is most suitable for the particular experiment. In the configuration that we used for the present work, a pair of 90°-off-axis parabolic mirrors collects thermally emitted radiance from a circular area of 1.5 mm in diameter on the sample and focuses it on the optical fiber. The radiance that is transmitted by the fiber to the detector unit is then spectrally split, using dichroic beamsplitters, into four beams and detected by an equal number of fast, LN_2-cooled InSb photodiodes. The four channels are nominally centered at 1.77, 2.27, 3.51, and 4.82 μm. Their respective spectral bandwidths (FWHM) are 0.26, 0.62, 0.74, and 1.1 μm. The pyrometer is capable of measuring radiance temperature in the four wavelength bands with a time resolution of 20 ns. However, a sampling interval of 0.1 ms per data point was sufficiently short for the melting experiments presented here. The blackbody-temperature threshold of the pyrometer is at about

350 K. More details on this instrument in a slightly different configuration can be found in Ref. 15.

3. DATA REDUCTION

3.1. Radiance Temperature

The pyrometer is calibrated by means of a blackbody furnace at some reference temperature T_{ref}. The radiance temperature $T_\lambda(t)$, as a function of time t, of a pulse-heated sample can then be computed by numerically solving

$$\frac{S\left(T_\lambda\left(t\right)\right)}{S\left(T_{\mathrm{ref}}\right)} = \frac{\int\limits_{\Delta\lambda} R_L\left(\lambda\right)_{\mathrm{p.n.}} L_{\lambda,\mathrm{b}}\left(\lambda, T_\lambda\left(t\right)\right) d\lambda}{\int\limits_{\Delta\lambda} R_L\left(\lambda\right)_{\mathrm{p.n.}} L_{\lambda,\mathrm{b}}\left(\lambda, T_{\mathrm{ref}}\right) d\lambda} \tag{1}$$

for each channel with sufficient signal. In the above equation S is the output signal as a function of radiance temperature, $R_L\left(\lambda\right)_{\mathrm{p.n.}}$ is the channel's peak-normalized spectral-radiance responsivity[5] as a function of wavelength λ, $L_{\lambda,\mathrm{b}}$ is the blackbody spectral radiance as given by Planck's law, and $\Delta\lambda$ is the wavelength interval over which the channel responsivity, as expressed by $R_L(\lambda)_{\mathrm{p.n.}}$, is significantly non-zero. The spectral-radiance responsivity of each channel in the range of 400 to 6000 nm was determined in a separate measurement using an automated monochromator system.

The melting-point radiance temperatures for a given sample are determined by averaging the measured radiance temperatures along the melting plateau of each channel. The melting-point radiance temperatures for each metal are, in turn, determined by averaging the results for several samples.

The wavelength corresponding to the melting-point radiance temperature $T_{\lambda,\mathrm{m}}$ in each channel is the mean effective wavelength $\lambda_{T_{\lambda,\mathrm{m}}-T_{\mathrm{ref}}}$ of that channel between $T_{\lambda,\mathrm{m}}$ and T_{ref}, as defined in Ref. 17:

$$\frac{S\left(T_{\lambda,\mathrm{m}}\right)}{S\left(T_{\mathrm{ref}}\right)} = \frac{\exp\left(\frac{c_2}{\lambda_{T_{\lambda,\mathrm{m}}-T_{\mathrm{ref}}} T_{\mathrm{ref}}}\right) - 1}{\exp\left(\frac{c_2}{\lambda_{T_{\lambda,\mathrm{m}}-T_{\mathrm{ref}}} T_{\lambda,\mathrm{m}}}\right) - 1}. \tag{2}$$

[5]The spectral-radiance responsivity can be expressed as the product of the throughput of the beam (its geometric extent) that is collected by the front-optics into the optical fiber, the spectral propagance of the entire path from the object to the detector, and the spectral-flux responsivity of the detector. The spectral propagance is the fraction of incident flux that is (successfully) propagated over an extended path [16]. It includes the attenuation due to all transmittances and reflectances over the entire path.

$S(T_{\lambda,\mathrm{m}})$ denotes the overall average of the average signals measured along the melting plateaus, in each channel, of several samples.

All temperatures reported in this paper are consistent with the definition of the International Temperature Scale of 1990 above the silver point [18].

3.2. Normal Spectral Emittance

The normal spectral emittance $\varepsilon_{\lambda,\mathrm{m}}$ at the melting point of each metal is determined, in each channel, from the ratio of the measured signal along the melting plateau and the expected signal for a blackbody at the known (true) melting temperature T_{m} of the metal:

$$\varepsilon_{\lambda,\mathrm{m}} = \frac{S\left(T_{\lambda,\mathrm{m}}\right)}{S\left(T_{\mathrm{m}}\right)} \quad \text{with} \quad S\left(T_{\mathrm{m}}\right) = S\left(T_{\mathrm{ref}}\right) \frac{\int_{\Delta\lambda} R_L\left(\lambda\right)_{\mathrm{p.n.}} L_{\lambda,\mathrm{bb}}\left(\lambda, T_{\mathrm{m}}\right) d\lambda}{\int_{\Delta\lambda} R_L\left(\lambda\right)_{\mathrm{p.n.}} L_{\lambda,\mathrm{bb}}\left(\lambda, T_{\mathrm{ref}}\right) d\lambda}. \tag{3}$$

The wavelength corresponding to the normal spectral emittance in each channel is the mean effective wavelength $\lambda_{T_{\lambda,\mathrm{m}}-T_{\mathrm{m}}}$ of that channel between $T_{\lambda,\mathrm{m}}$ and T_{m}, as defined in Ref. 17:

$$\varepsilon_{\lambda,\mathrm{m}} = \frac{\exp\left(\frac{c_2}{\lambda_{T_{\lambda,\mathrm{m}}-T_{\mathrm{m}}} T_{\mathrm{m}}}\right) - 1}{\exp\left(\frac{c_2}{\lambda_{T_{\lambda,\mathrm{m}}-T_{\mathrm{m}}} T_{\lambda,\mathrm{m}}}\right) - 1}. \tag{4}$$

It should be noted here that Eqs. (3) and (4) are not strictly correct unless the object viewed by the pyrometer is a graybody across the spectral passband $\Delta\lambda$ of each channel.[6]

4. MEASUREMENTS

Measurements of the radiance temperatures of the investigated metals at their melting points were performed on samples in the form of strips that were cut from 50 mm × 50 mm foils. The strips were 50 mm in length and 7 mm in width. The length of the strips that was actually heated was

[6] In any other case, $\varepsilon_{\lambda,\mathrm{m}}$ and T_{m} in Eq. (3) would have to be replaced by an equivalent graybody emittance ε_{g} and a corresponding graybody temperature T_{g}, respectively [17, 19]. Equation (4) would also have to be modified accordingly. However, ε_{g} and T_{g} may not exist and in any case cannot be computed exactly without advance knowledge of $\varepsilon_{\lambda,\mathrm{m}}$ as a function of wavelength across $\Delta\lambda$. It is doubtful that any attempt to approximate them in some way would enhance the accuracy, compared to simply using Eqs. (3) and (4).

shorter by a few millimeters, because both ends were clamped in the sample holder during the experiments. The purity of the materials (by mass), as reported by the manufacturer, was 99.99+% for the tin foil, 99.95+% for the zinc foil, 99.0% for the aluminum foil, and 99.95+% for the silver foil.

An integrating-sphere reflectometer, constructed at LANL, was used to measure the initial (prior to heating) normal spectral emittance of the samples at 1.55 μm in order to uncover any possible correlation between the initial surface roughness of the samples and the measured melting-point radiance temperatures. More details about the reflectometer and its operation can be found in Ref. 20.

Before each measurement the experiment chamber was evacuated to below 4 Pa and then back-filled with argon to a pressure slightly above atmospheric. This was done to reduce the rate of evaporation from the samples and, as a consequence, coating of the chamber windows. The pyrometry window was examined after each experiment and replaced when damage from some piece of the molten sample was observed.

Figure 1 shows typical radiance temperature data. In the case of tin, the signal in the shortest wavelength channel was not sufficient to be used. The flat region along each plateau was used to determine the melting radiance temperature at each wavelength. The radiance temperature along this flat region was essentially constant to better than ± 1 K in all cases.

4.1. Tin

Seven melting experiments were conducted on 0.50 mm-thick tin strips in the 'as received' condition. Well-formed melting plateaus were observed in all of them. The electrical current pulse, used to heat each sample from room temperature to its melting point, ranged in amplitude from 360 to 369 A. The samples reached their melting point in 216 to 256 ms, corresponding to average heating rates of 2.34 to 1.97 $K \cdot ms^{-1}$. The time from the onset of melting to the collapse of the partly liquid sample, as indicated by the abrupt loss of electrical continuity and the resulting end of the quasi-rectangular current pulse, ranged from 41 to 68 ms. The number of temperature-data points along the plateau used for averaging ranged from 151 to 451, depending on the melting behavior of the sample and on the wavelength. The standard deviation of an individual temperature-data point from the average plateau temperature of a sample was less than 3 K at the shortest wavelength with sufficient signal and less than 0.4 K at the longer ones.

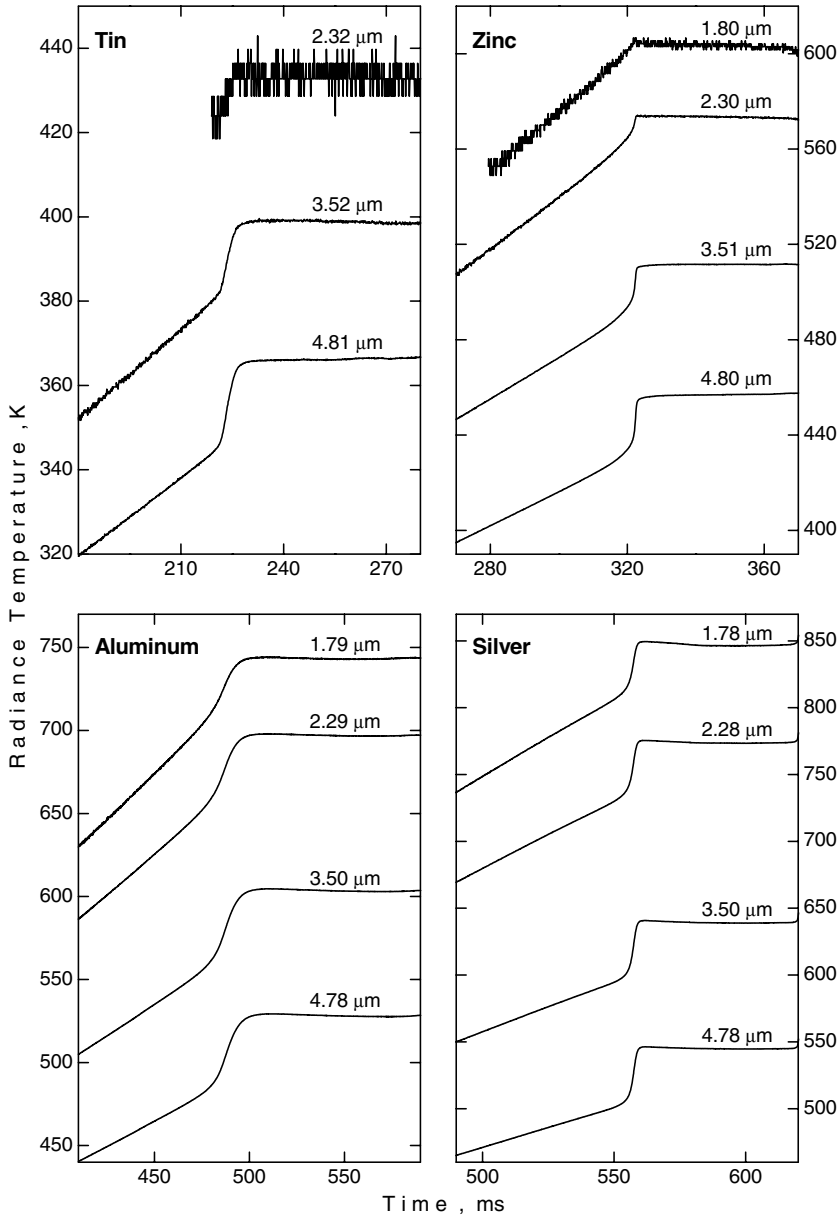

Fig. 1. Variation of the radiance temperatures of a tin, zinc, aluminum, and silver sample just before and during melting, as measured by the four-wavelength pyrometer.

4.2. Zinc

Well-formed melting plateaus were observed in ten out of eleven melting experiments that were conducted on 0.25 mm-thick zinc strips. In the one unsuccessful experiment, the sample broke apart at the onset of melting, probably because of extensive tension on the expansion joint of the sample holder. All samples were used in the 'as received' condition. The electrical current pulse, used to heat each sample from room temperature to its melting point, ranged in amplitude from 217 to 358 A. The samples reached their melting point in 315 to 852 ms, corresponding to average heating rates of 2.20 to 0.813 $K \cdot ms^{-1}$. The time from the onset of melting to the collapse of the partly liquid sample ranged from 57 to 153 ms. The number of temperature-data points along the plateau used for averaging ranged from 71 to 1001, depending on the heating rate, the melting behavior of the sample, and the wavelength. The standard deviation of an individual temperature-data point from the average plateau temperature of a sample was less than 1.2 K at the shortest wavelength and less than 0.4 K at the longer ones.

4.3. Aluminum

Seven melting experiments were conducted on 0.20 mm-thick aluminum strips in the 'as received' condition. Well-formed melting plateaus were observed in all of them. The electrical current pulse, used to heat each sample from room temperature to its melting point, ranged in amplitude from 369 to 377 A. The samples reached their melting point in 460 to 490 ms, corresponding to average heating rates of 2.03 to 1.91 $K \cdot ms^{-1}$. The time from the onset of melting to the collapse of the partly liquid sample ranged from 110 to 116 ms. The number of temperature data points along the plateau used for averaging ranged from 101 to 251, depending on the melting behavior of the sample and on the wavelength. The standard deviation of an individual temperature data point from the average plateau temperature of a sample was less than 0.15 K at all wavelengths.

4.4. Silver

Seven melting experiments were conducted on 0.15 mm-thick silver strips and three on 0.25 mm-thick strips. Well-formed melting plateaus were observed in all of them. However, in one case the measured signals exceeded the average melting-point signals by ten times the standard deviation of the remaining experiments from their average. Even though we did not have a plausible explanation for this behavior, we considered

this measurement an outlier and excluded it from further analysis of the results. The electrical current pulse, used to heat each sample from room temperature to its melting point, ranged in amplitude from 367 to 774 A. The melting point was reached in 130 to 587 ms, corresponding to average heating rates of 9.50 to 2.10 $K \cdot ms^{-1}$. The time from the onset of melting to the collapse of the partly liquid sample ranged from 14 to 75 ms. The number of temperature data points along the plateau used for averaging ranged from 111 to 221, depending on the heating rate, the melting behavior of the sample, and the wavelength. The standard deviation of an individual temperature data point from the average plateau temperature of a sample was less than 0.5 K at all wavelengths. Seven of the silver samples were used in the 'as received' condition and three were mechanically treated with 320-grit SiC abrasive paper in an effort to increase their normal spectral emittance by roughening their surfaces and to investigate the effect of this increase, if any, on the measured melting-point radiance temperatures.

5. RESULTS

The final results on the measured melting-point radiance temperatures and normal spectral emittances of tin, zinc, aluminum, and silver are presented in Table I and plotted as functions of wavelength in Figs. 2 and 3. The true melting temperatures that were used in computing the normal spectral emittances were 505.08 K for tin, 692.68 K for zinc, 933.47 K for aluminum, and 1234.93 K for silver [18].

Depending on the wavelength, the standard deviation of the average plateau radiance temperature of an individual sample from the overall average of several samples was in the range of 0.8 to 1 K for tin, 7 to 9 K for zinc, 0.8 to 1 K for aluminum, and 2 to 5 K for silver. Similarly, depending on the wavelength, the maximum absolute deviation of the average plateau radiance temperature of an individual sample from the overall average of several samples was in the range of 1.2 to 1.6 K for tin, 12 to 14 K for zinc, 1.6 to 2.1 K for aluminum, and 2 to 7 K for silver. Figures 4 and 5 show the deviation of the average plateau radiance temperatures of the individual samples from the final results.

6. DISCUSSION

Our measurements show that both the radiance temperature and the normal spectral emittance at the melting point of tin, zinc, aluminum, and silver decrease with increasing wavelength in the nominal range of 1.5 to 5 μm (Figs. 2 and 3). This finding is in agreement with previous

Table I. Radiance Temperature $T_{\lambda,\mathrm{m}}$ and Normal Spectral Emittance $\varepsilon_{\lambda,\mathrm{m}}$ (at the respective Mean Effective Wavelengths $\lambda_{T_{\lambda,\mathrm{m}}-T_{ref}}$ and $\lambda_{T_{\lambda,m}-T_{\mathrm{m}}}$) of Tin, Zinc, Aluminum, and Silver at Their Melting Points

Material and true melting temp. [18]	$\lambda_{T_{\lambda,\mathrm{m}}-T_{\mathrm{ref}}}$ (nm)[a]	$T_{\lambda,\mathrm{m}}$ (K)	S.D. (K)[b]	Max. abs. dev. (K)[c]	$\lambda_{T_{\lambda,\mathrm{m}}-T_m}$ (nm)[d]	$\varepsilon_{\lambda,\mathrm{m}}$ (−)	$\varepsilon_\ell/\varepsilon_s$ (−)[e]
Tin (7 samples)	2320	433.9	1	1.6	2370	0.139	–
T_m = 505.08 K	3524	399.6	0.9	1.3	3551	0.120	1.56
	4810	367.0	0.8	1.2	4845	0.109	1.62
Zinc (10 samples)	1795	606.3	7	12	1815	0.196	
T_m= 692.68 K	2300	577.5	8	13	2334	0.170	
	3514	517.1	9	14	3533	0.136	
	4796	463.3	9	14	4816	0.117	
Aluminum (7 samples)	1787	742.6	1	2.1	1792	0.110	1.51
T_m= 933.47 K	2285	696.6	0.8	1.6	2297	0.102	1.53
	3502	603.0	0.9	1.8	3505	0.0889	1.54
	4781	527.7	0.9	1.7	4784	0.0809	1.53
Silver (9 samples)	1784	846.8	5	7	1784	0.0501	1.53
T_m= 1234.93 K	2279	773.7	4	6	2280	0.0473	1.54
	3499	639.6	2	4	3496	0.0434	1.56
	4778	545.6	2	2	4773	0.0420	1.57

[a] Mean effective wavelength (as defined in Ref. 17) between $T_{\lambda,\mathrm{m}}$ and the calibration temperature T_{ref}.

[b] Standard deviation of the average plateau radiance temperature of an individual sample from the overall average of several samples.

[c] Maximum absolute deviation of the average plateau radiance temperature of an individual sample from the overall average of several samples.

[d] Mean effective wavelength (as defined in Ref. 17) between $T_{\lambda,\mathrm{m}}$ and the true melting temperature T_m.

[e] Ratio of the normal spectral emittance ε_ℓ in the liquid phase to that in the solid ε_s at the melting temperature.

work on higher-temperature metals by the thermophysics laboratories of the NIST and the IMGC [21].

Even though our investigation was limited in scope, there was no indication to suggest that the measured melting-point radiance temperatures depend on the applied heating rate. In the case of tin, silver, and aluminum there was no evidence of a trend in the measured values with respect to the initial surface roughness of the samples, either. This was particularly true in the case of the silver samples whose initial normal spectral emittance, as measured with our integrating-sphere reflectometer at 1.55 μm, was increased by a factor of at least two by mechanically

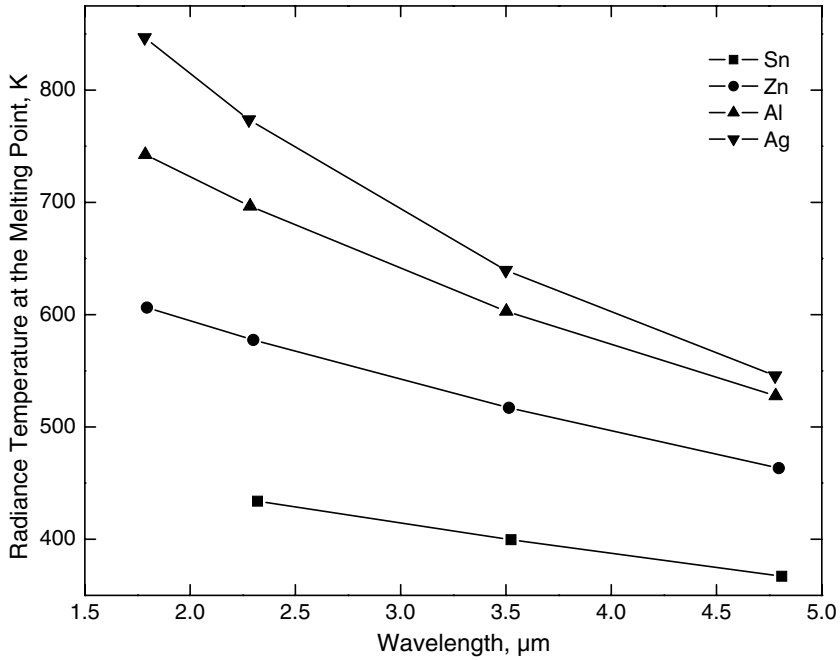

Fig. 2. Variation of the radiance temperature of tin, zinc, aluminum, and silver at their melting points as a function of wavelength.

abrading them prior to heating (Fig. 5). Zinc, however, exhibited a completely different behavior in the sense that a significant correlation was observed between the initial normal spectral emittance of the zinc samples and the measured melting-point radiance temperatures. Samples with a low initial emittance generally melted at lower radiance temperatures than those with higher initial emittance. This is clearly seen in Fig. 6 and explains the unusually large standard deviation between samples of the zinc results, as reported in Table I.

An interesting feature that was observed in these experiments was a sudden increase of the measured radiances at the onset of melting, which can also be seen in the radiance temperature traces shown in Fig. 1. In the case of tin this increase in radiance was on the order of 50 to 60% in the two longest wavelengths, whereas no discernible change was seen at the shorter wavelength. In the case of aluminum it was on the order of 50% at all wavelengths and in the case of silver it was on the order of 50 to 60% at all wavelengths. Again zinc stood out with its behavior compared to the other three investigated metals by exhibiting a large variation in the magnitude of this radiance increase. In particular, we could clearly distinguish

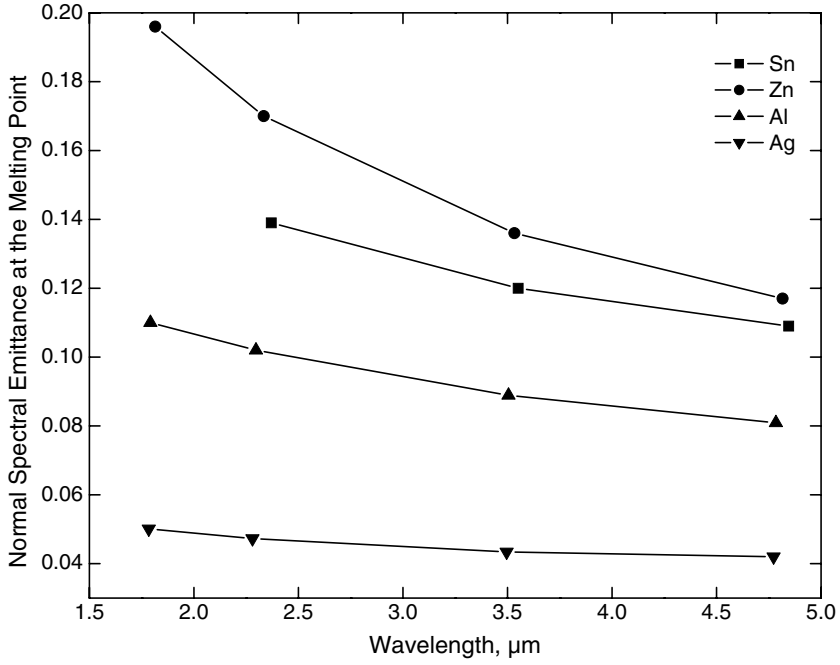

Fig. 3. Variation of the normal spectral emittance of tin, zinc, aluminum, and silver at their melting points as a function of wavelength.

between the samples with a low initial normal spectral emittance, whose melting-point radiance temperatures were also measured lower, and those with a higher initial emittance and the higher melting-point radiance temperatures. In the first group the increase was larger, around 12% at 2.3 μm, 25% at 3.5 μm, and 34% at 4.8 μm, whereas in the second it was around 3%, 9%, and 13% at the same wavelengths. As with tin, we did not observe an increase at the shortest wavelength.

We believe that this observed radiance increase at the onset of melting is caused by a change in the emittance of the samples and not a true temperature increase. Such a temperature increase, for which we cannot think of a reason, would have been accompanied by radiance increases in all channels. Moreover, it follows from Planck's law, that the relative increase in radiance caused by an increase in temperature should have been larger at the shorter wavelengths, which is not what we observed. It is conceivable that what we saw was initiation of melting on the surface of the samples [22] and that the increases in radiance are due to intrinsic differences between solid and liquid. In that case the relative signal changes

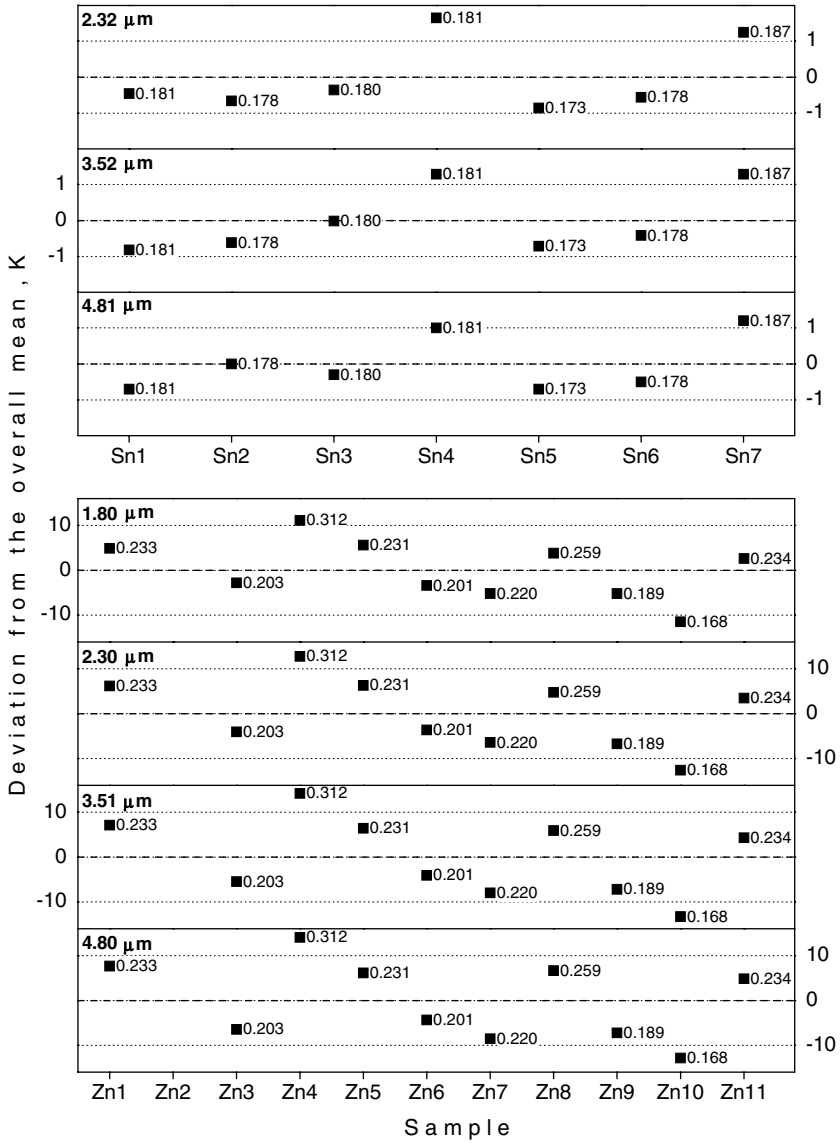

Fig. 4. Deviation of the measured radiance temperatures at the melting point of the individual tin and zinc samples from the overall mean values (represented by the 'zero' lines) at four wavelengths. The numbers next to the data points indicate the initial (prior to heating) normal spectral emittance of the samples, as measured with an integrating sphere reflectometer at 1.55 μm.

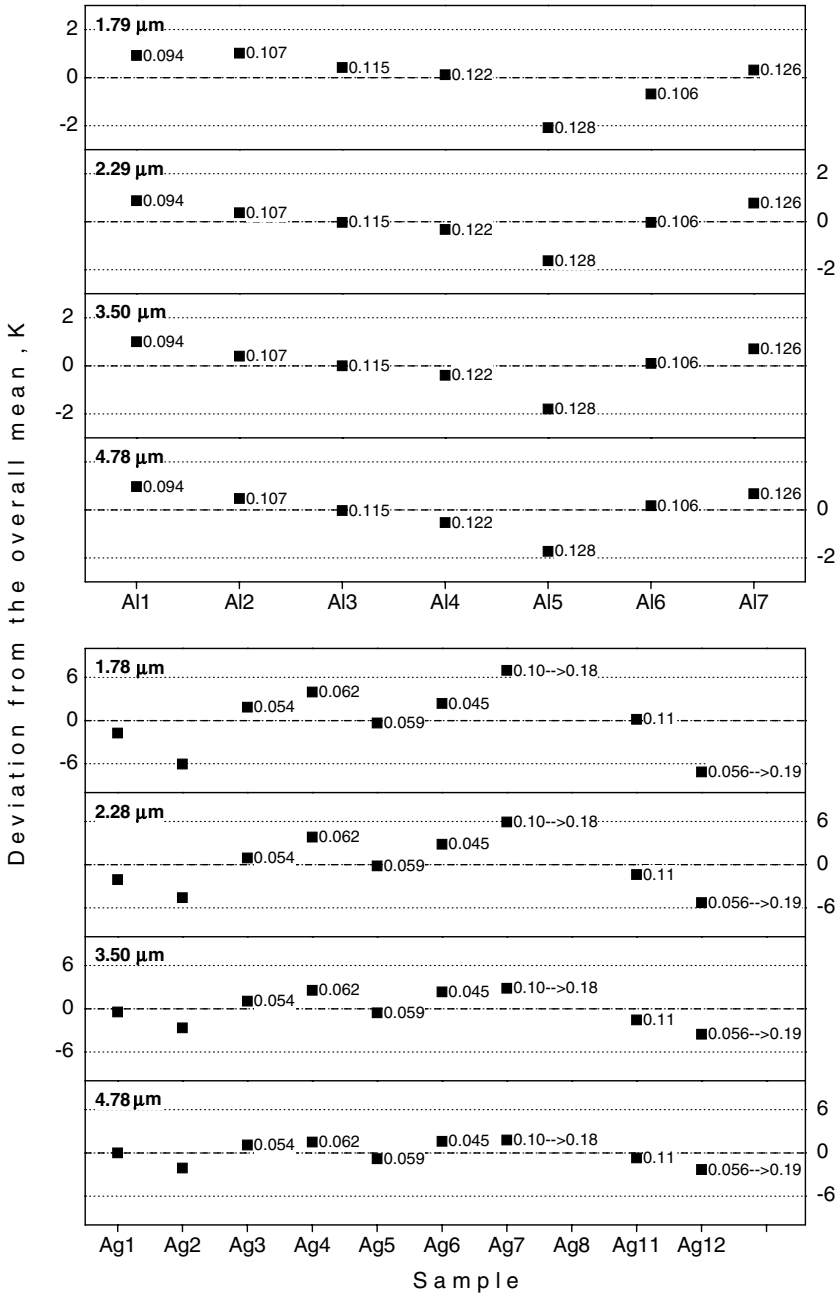
1.79 µm
2.29 µm
3.50 µm
4.78 µm
0.094
0.107
0.115
0.122
0.128
0.106
0.126
Al1
Al2
Al3
Al4
Al5
Al6
Al7
1.78 µm
2.28 µm
3.50 µm
4.78µm
0.054
0.062
0.059
0.045
0.10-->0.18
0.11
0.056-->0.19
Ag1
Ag2
Ag3
Ag4
Ag5
Ag6
Ag7
Ag8
Ag11
Ag12
Sample
Deviation from the overall mean, K

◀

Fig. 5. Deviation of the measured radiance temperatures at the melting point of the individual aluminum and silver samples from the overall mean values (represented by the 'zero' lines) at four wavelengths. The numbers next to the data points indicate the initial (prior to heating) normal spectral emittance of the samples, as measured with an integrating sphere reflectometer at 1.55 μm. In the case of the silver samples whose surface was roughened with abrasives prior to pulse-heating them, an arrow is used to point out the change in their normal spectral emittance caused by this treatment and both emittance values (before and after the treatment) are given.

are equal to relative emittance changes between solid and liquid. These ratios are reported in Table I. A roughening of the surface is unlikely because one expects the surface to smoothen due to surface tension at the onset of melt. In addition, the shorter wavelength channels would, presumably, have been more sensitive to such an increase in roughness. It would be interesting to correlate these radiance increases, at least in part, with changes in the resistivity of the materials as they melt by using a simplified relation between emittance and resistivity such as that of Hagen

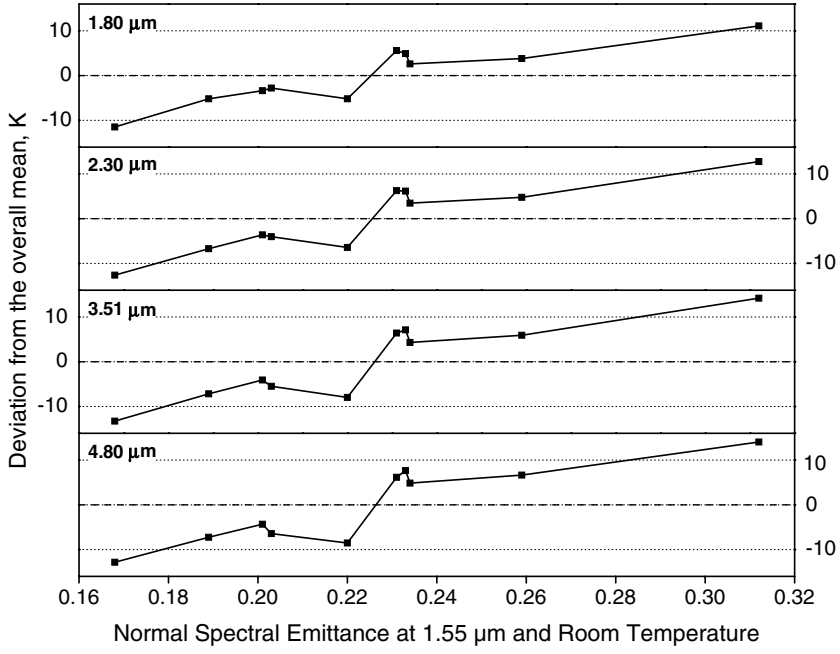

Fig. 6. Deviation of the measured radiance temperatures at the melting point of the individual zinc samples from the overall mean values (represented by the 'zero' lines) as a function of the initial (prior to heating) normal spectral emittance of the samples at 1.55 μm.

and Rubens [23]. In any case, more research is needed to fully explain our observation.

REFERENCES

1. A. Cezairliyan, A. P. Miiller, F. Righini, and A. Rosso, in *Temperature: Its Measurement and Control in Science and Industry*, Vol. 5, Part 1, J. F. Schooley, ed. (AIP, New York, 1982), p. 377.
2. A. Cezairliyan, G. M. Foley, M. S. Morse, and A. P. Miiller, in *Temperature: Its Measurement and Control in Science and Industry*, Vol. 6, Part 2, J. F. Schooley, ed. (AIP, New York, 1992), p. 757.
3. A. P. Miiller and A. Cezairliyan, *Int. J. Thermophys*. **14**:511 (1993).
4. A. Cezairliyan, J. L. McClure, and A. P. Miiller, *High Temp. High Press*. **25**:649 (1993).
5. A. Cezairliyan, J. L. McClure, and A. P. Miiller, *Int. J. Thermophys*. **15**:993 (1994).
6. J. L. McClure and A. Cezairliyan, *Int. J. Thermophys*. **18**:291 (1997).
7. E. Kaschnitz and A. Cezairliyan, *Int. J. Thermophys*. **17**:1069 (1996).
8. E. Kaschnitz, J. L. McClure, and A. Cezairliyan, *Int. J. Thermophys*. **19**:1637 (1998).
9. J. L. McClure, K. Boboridis, and A. Cezairliyan, *Int. J. Thermophys*. **20**:1137 (1999).
10. J. L. McClure, A. Cezairliyan, and E. Kaschnitz, *Int. J. Thermophys*. **20**:1149 (1999).
11. K. Boboridis, A. Seifter, A. W. Obst, and D. Basak, presented at the *15th Symp. Thermophys. Props.*, Boulder, Colorado (2003).
12. A. Cezairliyan, M. S. Morse, H. A. Berman, and C. W. Beckett, *J. Res. Nat. Bur. Stand. (U.S.)* **74A**:65 (1970).
13. A. Cezairliyan, *J. Res. Nat. Bur. Stand. (U.S.)* **75C**:7 (1971).
14. T. Matsumoto and A. Cezairliyan, *Int. J. Thermophys*. **18**:1539 (1997).
15. K. Boboridis and A. W. Obst, in *Temperature: Its Measurement and Control in Science and Industry*, Vol. 7, Part 2, D. C. Ripple, ed. (AIP, New York, 2003), p. 759.
16. F. E. Nicodemus and H. J. Kostkowski, in *Self-Study Manual on Optical Radiation Measurements*, F. E. Nicodemus, ed., Nat. Bur. Stand. Tech. Note 910–1 (1976), p. 38.
17. H. J. Kostkowski and R. D. Lee, in *Temperature: Its Measurement and Control in Science and Industry*, Vol. 3, Part 1, C. M. Herzfeld, ed. (Reinhold, New York, 1962), p. 449.
18. H. Preston-Thomas, *Metrologia* **27**:3 (1990); *Metrologia* **27**:107 (1990).
19. G. D. Nutter, in *Theory and Practice of Radiation Thermometry*, D. P. DeWitt and G. D. Nutter, eds. (Wiley, New York, 1988), p. 302.
20. A. Seifter, K. Boboridis, and A. W. Obst, submitted to *Int. J. Thermophys*.
21. A. Cezairliyan, A. P. Miiller, F. Righini, and A. Rosso, *High Temp. High Press*. **23**:325 (1991).
22. J. G. Dash, *Contemp. Phys*. **30**:89 (1989).
23. E. Hagen and H. Rubens, *Ann. d. Physik*. **4**:873 (1903).